Biosensors and Bioelectronics 143 (2019) 111625

Contents lists available at ScienceDirect

Biosensors and Bioelectronics

journal homepage: www.elsevier.com/locate/bios

Immunodiagnostic of leprosy exploiting a photoelectrochemical platform based on a recombinant peptide mimetic of a *Mycobacterium leprae* antigen

Sakae Yotsumoto Neto[a], Mayara Ingrid Sousa Lima[b], Silma Regina Ferreira Pereira[b], Luiz Ricardo Goulart[c], Rita de Cássia Silva Luz[a], Flavio Santos Damos[a,*]

[a] Department of Chemistry, Federal University of Maranhão-UFMA, 65080-805, São Luís, MA, Brazil
[b] Department of Biology, Federal University of Maranhão-UFMA, 65080-805, São Luís, MA, Brazil
[c] Institute of Genetics and Biochemistry, Federal University of Uberlândia, Uberlândia, MG, Brazil

ARTICLE INFO

Keywords:
Leprosy
Recombinant mimetic peptide
Photoelectrochemical immunosensor
Mycobacterium leprae
Visible LED light

ABSTRACT

The first serum diagnosis of leprosy based on the detection of antibodies of patients using a recombinant mimetic peptide (PGL1M3R) as recognition element and exploiting a photoelectrochemical sensor is presented in this work. The photoeletrochemical platform consists of cadmium sulphide and nickel hydroxide electrodeposited on fluorine-doped tin oxide coated glass slide (CdS/$Ni(OH)_2$/FTO). The optical band gap and flat band potential of the photoelectroactive materials were evaluated by UV–Vis spectroscopy and electrochemical impedance spectroscopy. The spatial photoelectrochemical response of the platform was evaluated by Scanning Electrochemical Microscopy and the morphology of the films was investigated by Scanning Electron Microscopy (SEM). The photoelectrochemical response of the CdS/$Ni(OH)_2$/FTO platform was optimized by evaluating the effects of the kind, concentration, and pH of the buffer. Furthermore, the applied potential to the CdS/$Ni(OH)_2$/FTO platform was also investigated. The CdS/$Ni(OH)_2$/FTO photoelectrochemical platform was modified with a synthetic peptide by using glutaraldehyde as cross-linking reagent and chitosan (CS) for the covalent coupling of the peptide to the photoelectrochemical platform (PGL1M3R/CdS/$Ni(OH)_2$/FTO). The photoelectrochemical immunosensor is able to distinguishing between positive and negative leprosy human sera samples diluted from 1:640 up to 1:10240. Furthermore, to test the specificity of the sensor, samples from tuberculosis and leishmaniasis patients were analyzed using the proposed photoelectrochemical immunosensor.

1. Introduction

Leprosy is a disabling chronic infectious disease caused by the bacillus *Mycobacterium leprae* that affects the skin and peripheral nerves. It has a wide spectrum of clinical-pathologic features depending on the cellular and humoral immunity and it remains a public health challenge in many developing countries (Wheeler et al., 2017).

According to reports received from 138 countries from World Health Organization regions, the global registered prevalence of leprosy at the end of 2016 was 214 783 cases. In addition, the number of newly-detected cases of leprosy reported globally in 2015 and 2014 were 211 973 and 213 899, respectively, which indicates the high rate of continued transmission of infection by *M. leprae* (WHO, 2017). Among the more important actions to reduce the rate of new cases of leprosy is the early diagnosis to provide a prompt treatment (Rodrigues and Lockwood, 2011). In addition, the monitoring of patients under treatment and their contactants is essential for the interruption of the chain of transmission of the bacillus and for the reduction of drug resistance.

According to the Ridley-Jopling criteria (Ridley and Jopling, 1962, 1966), the leprosy patients can be classified as tuberculoid (TT), borderline-tuberculoid (BT), borderline-borderline (BB), borderline-lepromatous (BL), and lepromatous (LL) indicating a wide spectrum of clinical forms of the disease and whose detection is usually based on clinical signs and symptoms (Lobato et al., 2011).

Therefore, the diagnosis of leprosy is difficult requiring skilled professionals to discriminate each case of leprosy from some other diseases such as hypochromic eczematides, tinea corporis, vitiligo, among others such as there is not gold standard diagnostic test (Yang et al., 2013). Thus, the development of diagnostic laboratory tests that helps health professionals to confirm the disease at an early stage among symptomatic patients can be helpful to the establishment of an appropriate treatment. In this sense, the development of novel serological diagnostic methods figures out as an interesting and complementary alternative for the leprosy diagnosis since presence of some

* Corresponding author.
E-mail address: flavio.damos@ufma.br (F.S. Damos).

https://doi.org/10.1016/j.bios.2019.111625
Received 26 June 2019; Received in revised form 14 August 2019; Accepted 21 August 2019
Available online 22 August 2019
0956-5663/

circulating antibodies has been correlated with the clinical spectrum and bacterial index in leprosy patients (Lobato et al., 2011).

Nowadays, the enzyme-linked immunosorbent assay (ELISA) and immunochromatographic (lateral flow) are between the most common serological techniques employed to leprosy determination (Alban et al., 2014; Duthie et al., 2014a,b; Jadhav et al., 2011). Although these methods become selective, sensitive and reproductive serological tests, they require several steps to be performed presenting parts which are not of simple reduction of dimension to a single platform of detection. Thus, the proposition of novel strategies for more simple, cheap, sensitive and specific diagnostic tests with high throughput screening for the determination of leprosy is highly desirable to monitor the early cases, transmission and dissemination of this disease.

Among the most cheap, portable, and prominent methods for the serological diagnostic hangs out the photoelectrochemical devices (Liu and Jiang, 2017; Yotsumoto et al., 2018) since they can operate exploiting energy from the light of the environment to generate photocurrent as analytical signal (Zhao et al., 2015). The photoelectrochemical platforms exploits semiconducting based materials since they are frequently highly photoactive being excellent materials for the immobilization of antigens and antibodies (Yotsumoto et al., 2017). Some properties of these semiconducting based materials such as its photoluminescence, molar absorption coefficients, fluorescence quantum yields, and capability to generate electron-role couples are highly affected by biological reactions as immunoreactions between antigens and antibodies, enzymes and substrates, among others (Zhang et al., 2017).

Cadmium sulfide presents a conduction band at about −1 V *vs* normal hydrogen electrode, optical band gap of 2.4 eV, high electron density at room temperature, and large exciton binding energy (Tang et al., 2015). In this sense, CdS has been exploited in development of novel photocatalists, photovoltaic based devices, photodetectors, and photoelectrochemical sensors (Wang et al., 2015).

Although the cadmium sulfide become a profitable photoactive material, it shows some limitations such as high rate of electron-hole recombination and its susceptibility to photocorrosion in aqueous solution when photo-induced reactions of the CdS itself can be oxidized by the photogenerated holes such as cadmium sulfide has been combined to semiconductors, conducting polymers, graphene, and metal nanoparticles (Yotsumoto et al., 2017; Feng et al., 2017). In this sense, nickel hydroxide-based materials stand out as an interesting strategy to reduce the electron-hole recombination and alleviating the effects of the photogenerated holes on CdS itself since $Ni(OH)_2$/NiOOH and Ni $(OH)_2$/Ni redox couples present excellent electrocatalytic and redox-mediating properties (Bora et al., 2013).

Although many interesting chemical routes, such as sonochemistry, sol gel, solvothermal methods, among others, have been described for the formation of cadmium sulfide and nickel hydroxide on surfaces (Mao et al., 2019; Vamvasakis et al., 2018; Wang et al., 2017), the direct formation of particles *in situ* on the electrode support of interest by electrodeposition is a simple alternative to chemical methods. Therefore, the present work describes the development and application of a novel CdS/$Ni(OH)_2$/FTO photoelectrochemical sensor for the detection of leprosy exploiting a peptide-based antigen of leprosy. To the best of our knowledge, this is the first photoelectrochemical immunosensor for the identification of positive and negative cases of leprosy exploiting a visible light-emitting diode light as excitation source.

2. Materials and methods

2.1. Reagents and solutions

All working solutions were prepared with reagents of high purity without further purification steps in deionized water from GEHAKA Company (Gehaka Ltd., São Paulo, SP, Brazil). Chitosan, cadmium chloride, nickel nitrate, sodium thiosulfate, glutaraldehyde, and bovine serum albumin (BSA) were purchased from Sigma-Aldrich (St. Louis, MO, USA). Ammonium chloride, hydrochloric acid, sodium hydroxide, ethanol, monobasic sodium phosphate, dibasic sodium phosphate, and citric acid were purchased from Isofar (Rio de Janeiro, RJ, Brazil).

2.2. Morphological, electrochemical and UV–Visible spectroscopy measurements

The morphology of the CdS/FTO, $Ni(OH)_2$/FTO, and CdS/$Ni(OH)_2$/FTO were investigated by scanning electron microscopy (SEM). SEM images were obtained using a Quanta 3D FEG-FEI operated at an accelerating potential of 5.00 kV. EDX analysis were performed with an EDX XFLASH detector from Bruker.

The photoelectrochemical measurements were carried out in a made home box to control the light incidence on the photoactive platform. The acquisition of photocurrent was performed with aid of a three-electrode electrochemical cell with a fluorine doped tin oxide-coated glass substrate (FTO) as working electrode, an Ag/AgCl (saturated KCl) as reference electrode and a platinum wire was employed as counter electrode. A potentiostat/galvanostat model PGSTAT 128N equipped with a frequency response analyser module from Metrohm-Autolab B.V. (Utrecht, the Netherlands) was employed for data acquisition. The Nyquist and Bode-phase spectra were performed in the frequency ranging from 10^5 Hz to 10^{-1} Hz under AC voltage amplitude of 10 mV.

Scanning electrochemical microscopy (SECM) images were performed with a Sensolytics base (Bochum, Germany). The SECM measurements were performed with aid of a platinum microelectrode of 25 μm diameter. The SECM images were performed in a three electrode electrochemical cell assembled on top of the CdS/$Ni(OH)_2$/FTO surface. The electrolyte was a solution containing 5 mmol L^{-1} $[Fe(CN)_6]^{3-}$ and 0.1 mol L^{-1} KCl. The approach of the SECM microelectrode to the unbiased CdS/$Ni(OH)_2$/FTO surface was performed biasing the tip at −200 mV *vs* Ag/AgCl.

A commercial parabolic aluminum reflector (PAR) based light emitting diode (LED) lamp of about 35 W was used as irradiation source in all photoelectrochemical measurements. Absorption spectra obtained from 280 to 1100 nm were performed with a spectrophotometer model AvaSpec/2048 from Avantes (The Netherlands).

The analytical response of the photoelectrochemical immunosensor to the samples was evaluated by incubating the surface of the immunosensor with 20 μL of solutions of serum samples at nine different dilutions (from 1:40 up to 1:10240) for 5 min. Finally, the surface of the photoelectrochemical sensor was washed before the photoelectrochemical measurements in the buffer solutions.

2.3. Construction of the photoelectrochemical immunosensor

The FTO electrode was washed and it was sonicated with ethanol and water to remove any previously adsorbed species. The electrodeposition and activation of the nickel-based film was performed from bath solutions containing 0.01 mol L^{-1} $Ni(NO_3)_2$ and 1 mol L^{-1} NH_4Cl biasing the FTO working electrode at −1.3 V *vs* Ag/AgCl under 120 s. Thereafter, the previously deposited nickel film was electrochemically activated by scanning the electrode potential between 0 and 0.8 V vs Ag/AgCl in 0.1 mol L^{-1} KOH at a scan rate of 50 mV s^{-1} (20 cycles) in order to produce the $Ni(OH)_2$.

The CdS film was electrodeposited from a platting solution containing 0.02 mol L^{-1} $CdCl_2$ and 0.1 mol L^{-1} sodium thiosulphate. The pH of the bath solution was adjusted with hydrochloric acid to 2.3 and 10 (ten) potential scans were performed between −1000 mV and 600 mV *vs* Ag/AgCl for the electrodeposition of CdS on $Ni(OH)_2$ modified FTO surface.

Finally, 22 μL of PGL1M3R peptide (100 μg mL^{-1}) was add to 23 μL of chitosan 1% and 10 μL of glutaraldehyde 0.5% to obtain 40 μg mL^{-1} of peptide solution. The photoelectrochemical sensor was produced by adding 20 μL of the peptide solution on the surface of the CdS/$Ni(OH)_2$/

FTO platform. Further, the PGL1M3R peptide modified photoelectrochemical sensor (PGL1M3R/CdS/$Ni(OH)_2$/FTO) was dried by evaporation at room temperature. In order to remove weakly adsorbed species, the surface of the peptide-modified photoelectrochemical sensor was thoroughly rinsed with phosphate buffer (0.1 mol L^{-1}, pH 7.4). Besides, the photoelectrochemical immunosensor was incubated with 20 μL of BSA/PBS (1%) for 20 min to avoid non-specific binding. Finally, the excess of BSA was removed by washing the sensor's surface (0.1 mol L^{-1} phosphate buffer, pH 7.4).

2.4. Patient accrual, sample collection and peptide synthesis

The PGL1M3R peptide used at this work was a synthetic peptide mimetic of the Phenolic glycolipid 1 (PGL-1) of the *Mycobacterium leprae* surface (NH3-HWMLPGGPPGGGPPHWMLPEDPPGGGPPHWFLWD-GPPGGGPPHWCLWDGPPGGGPPSSPIWPSPPGGGPPSMSRYGQ-CONH2), under the patent application BR 102014003636-9 A2). The chemical synthesis was performed by microwave-assisted peptide synthesis at the Peptide 2.0 Inc (Chantilly, VA, USA). The peptide C-terminus was amidated, and the final product was further analyzed and purified by HPLC.

The serum samples evaluated at this work were collected from individuals from São Luís city, Maranhão, Brazil, which is a hyperendemic region of leprosy. This study was performed according to recommendations of the "Guidelines of the National Board on Human Research Ethics" (CONEP) under approval of the Research Ethics Committee (CEP 449/10 and CAE 23115003005/2009-36). All the patients signed an informed consent form approved by the Research Ethics Committee on Humans from the Federal University of Maranhão, Brazil and their identities were kept anonymous throughout the study.

Positive samples were obtained from four patients with multibacillary leprosy, which have presented positive bacilloscopic index and positive serology for anti-PGL1. The negative samples were from four endemic controls, that is, the individuals living in the endemic area, but have never reported contact with leprosy patients. In addition, the endemic controls presented negative serology for anti-PGL1 based on ELISA (Enzyme-Linked Immunosorbent Assay) immunoassays.

The pools of serum samples from multibacillary patients and endemic controls were prepared by using 20 μL of serum of each individual. Thus, two pools were prepared, one positive pool sample for multibacillary patients and the other negative pool sample for endemic controls.

To evaluate the capacity of the photoelectrochemical immunosensor to recognize the presence of *M. leprae* antibodies in human serum, the photoelectrochemical immunosensor was incubated with 20 μL of each diluted sample (from 1:40 up to 1:10240) for 5 min. The photoelectrochemical sensor surface was rinsed using phosphate buffer solution (0.1 mol L^{-1}, pH 7.4) to leach out the excess of biological sample. Finally, the photoelectrochemical measurements were performed in a made home box to control the incidence of light on the sensor surface. A 35 W LED lamp was exploited as excitation source. Furthermore, to test the specificity of the sensor tuberculosis and leishmaniasis patients were analyzed using the proposed photoelectrochemical immunosensor.

3. Results and discussion

3.1. Characterization of the CdS/$Ni(OH)_2$/FTO photoelectrochemical platform

Scanning electron microscopy (SEM) analysis and energy-dispersive X-ray (EDX) spectroscopy measurements of the CdS/FTO, $Ni(OH)_2$/FTO, and CdS/$Ni(OH)_2$/FTO photoelectrodes were performed in order to evaluate the microscopic characteristics of the photoelectrodes (Fig. 1). As can be seen at Fig. 1(A), the SEM image of the surface of the CdS electrodeposited on fluorine doped tin oxide modified glass slide presents a sponge-like nanometric nodules of rough and irregular surface constituted of nanometric particles covering the surface of the FTO electrode and the EDX spectrum (Fig. 1(B)) presented mainly signals of Cd, S, Sn, Si, and O. The Cd/S ratio for the CdS films on FTO/glass substrate was about 1, which is the stoichiometric ratio expected to CdS. The Sn, Si, and O are due to the FTO/glass substrate.

The SEM image and EDX spectrum of $Ni(OH)_2$/FTO are presented in Fig. 1(C and D). Fig. 1(C) shows a non-compact distribution of grains due to the presence of $Ni(OH)_2$ particles. During the nickel electrodeposition, the metal reduction is accompanied of hydrogen evolution on the cathode surface. Thus, NH_4^+ species can act as buffer and hydrogen source suppressing changes of the pH at the cathode surface which can act improving the ability of the system to a more uniform nickel electrodeposition. The EDX spectrum (Fig. 1(D)) obtained for Ni $(OH)_2$/FTO presented peaks corresponding mainly to Ni, Sn, and O. Similarly to CdS electrodeposition, the presence of the oxygen and tin peaks in the $Ni(OH)_2$/FTO spectrum can be due to the FTO/glass substrate. The SEM image of CdS/$Ni(OH)_2$/FTO presented in Fig. 1(E) demonstrates a non-compact distribution of grains which can be due to the presence of CdS and $Ni(OH)_2$ particles. In addition, the agglomeration of grains of different sizes can be seen on the surface of the FTO electrode. On the other hand, the EDX spectrum of CdS/$Ni(OH)_2$/FTO (Fig. 1(F)) presented peaks corresponding to Cd, S, Ni, O, Sn, and Si which can be attributed to CdS, $Ni(OH)_2$ and FTO/glass substrate.

In order to monitor the optical characteristics of the photoactive materials, the optical band gap energy of $Ni(OH)_2$/FTO (blue line) and CdS/$Ni(OH)_2$/FTO (black line) were obtained from UV–Vis absorption spectra of each material (Fig. 2(A)) by using the following equation (Al-Hussam and Jassim, 2012):

$$(\alpha h\nu)^{1/n} = A(h\nu - E_g) \quad (1)$$

where 'α' is absorption coefficient $h\nu$ is the incident photon energy, E_g is the band gap energy, and $n = 1/2$ for direct bandgap materials such as CdS and $Ni(OH)_2$.

Thus, the band gap energy of each material was estimated by extrapolating the linear part of the curve to zero absorption ($\alpha = 0$) (Rodríguez et al., 2016) such as the optical band gap of the $Ni(OH)_2$/FTO and CdS/$Ni(OH)_2$/FTO were 3.13 eV and 2.19, respectively. As can be seen, it is observed that the absorption intensity of the composite in the visible region is higher than that observed to the $Ni(OH)_2$/FTO.

The electronic properties of the CdS/$Ni(OH)_2$/FTO, CdS/FTO, and $Ni(OH)_2$/FTO were evaluated by electrochemical impedance in 0.5 mol L^{-1} Na_2SO_4 as electrolyte solution. In this sense, the sensitivity of the CdS/$Ni(OH)_2$/FTO to presence/absence of light and the effects of the illumination on its electrochemical performance were evaluated in the absence of a hole scavenger (Fig. 2(B)). The Nyquist plots presented in Fig. 2(B) show that CdS/$Ni(OH)_2$/FTO platform is highly sensitive to illumination such as its charge transfer resistance significantly decreased in light conditions. The reduction of the charge transfer resistance indicates that CdS/$Ni(OH)_2$/FTO platform is highly efficient to generate electron/hole couples absorbing energy of the photons from the incoming LED light (Ooms et al., 2016).

Mott-Schottky analysis of the films were performed in order to evaluate charge transport at the junction, flat band potential (E_{fb}), and the effect of the charge carriers density (N). The capacitance of the photoanode-electrolyte junction in the photoelectrochemical cell was measured as a function of the electrode potential under dark condition at a fixed frequency of 500 Hz (Fig. 2(C)).

The Mott-Schottky (M-S) plot was performed by plotting C^{-2} versus the potential applied to the electrode and the M-S analysis was performed according to the following equation (Mott-Schottky equation) (Gelderman et al., 2007):

$$\frac{1}{C^2} = \pm\frac{2}{Ne\varepsilon_0\varepsilon}\left(E - E_{fb} - \frac{kT}{e}\right) \quad (2)$$

where e is the electron charge, C is the space charge capacitance in the semiconductor, ε_0 is the permittivity of the vacuum, ε is the relative

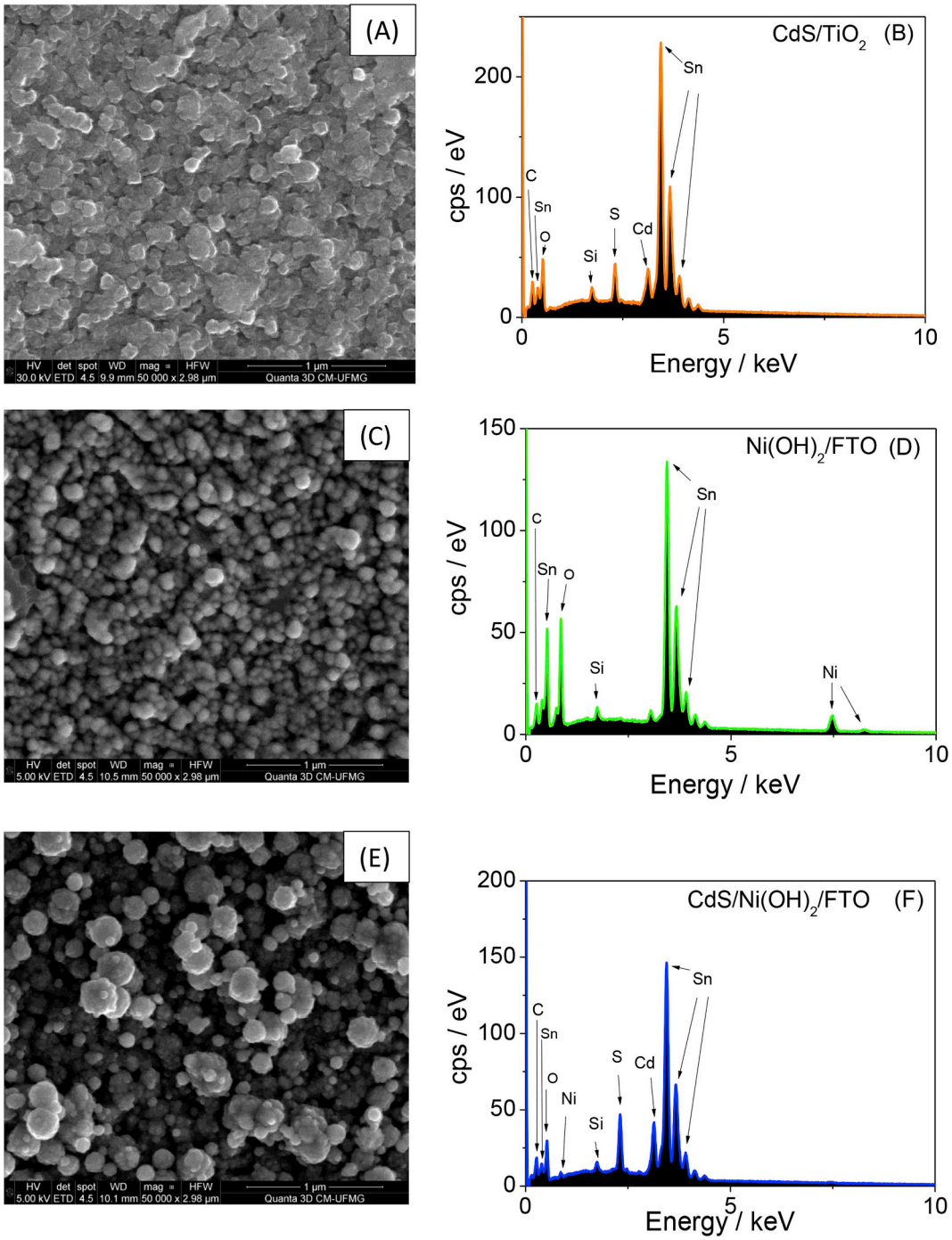

Fig. 1. SEM top view images and EDX spectra of CdS/FTO (A and B), $Ni(OH)_2$/FTO (C and D) and CdS/$Ni(OH)_2$/FTO (E and F) photoelectrodes.

permittivity of the semiconductor, N is the donor or acceptor carrier density, T is the absolute temperature, and k is the Boltzmann constant.

The slopes of the M-S plots for CdS/FTO and CdS/$Ni(OH)_2$/FTO were positive indicating n-type semiconductors. The slope of the M-S plot of CdS/$Ni(OH)_2$/FTO was 2.4 fold higher than that observed to CdS/FTO indicating that the interaction between cadmium sulfide and $Ni(OH)_2$ improves the carrier density and photoelectrochemical properties of the photoanode. In addition, flat band potential, determined from the intercept of the linear at $C^{-2} = 0$, was more negative for CdS/$Ni(OH)_2$/FTO ($E_{fb} = -1{,}4$ V) than that observed to CdS/FTO ($E_{fb} = -1{,}0$ V) indicating reduced recombination of excitons, better photoelectron lifetimes and transfer rates of photo-induced electrons (Izgorodin et al., 2009).

In order to evaluate the lifetime of the electron (τ_e) in conduction band of each material, the plot of the phase angle versus frequency for CdS/FTO, $Ni(OH)_2$/FTO, and CdS/$Ni(OH)_2$/FTO (Fig. 2(D)) was constructed and analyzed according to the following equation (Bisquert et al., 2009):

$$\tau_e = (2\pi f_{max})^{-1} \quad (3)$$

where f_{max} is the maximum frequency in the Bode phase plots. As can be seen, the estimated value of f_{max} in CdS/$Ni(OH)_2$/FTO was the lowest in Bode-phase plot indicating the better electron lifetime among the exploited materials.

Fig. 2(E) and (F) show the Scanning Electrochemical images obtained for CdS/$Ni(OH)_2$/FTO under incidence of visible LED light and

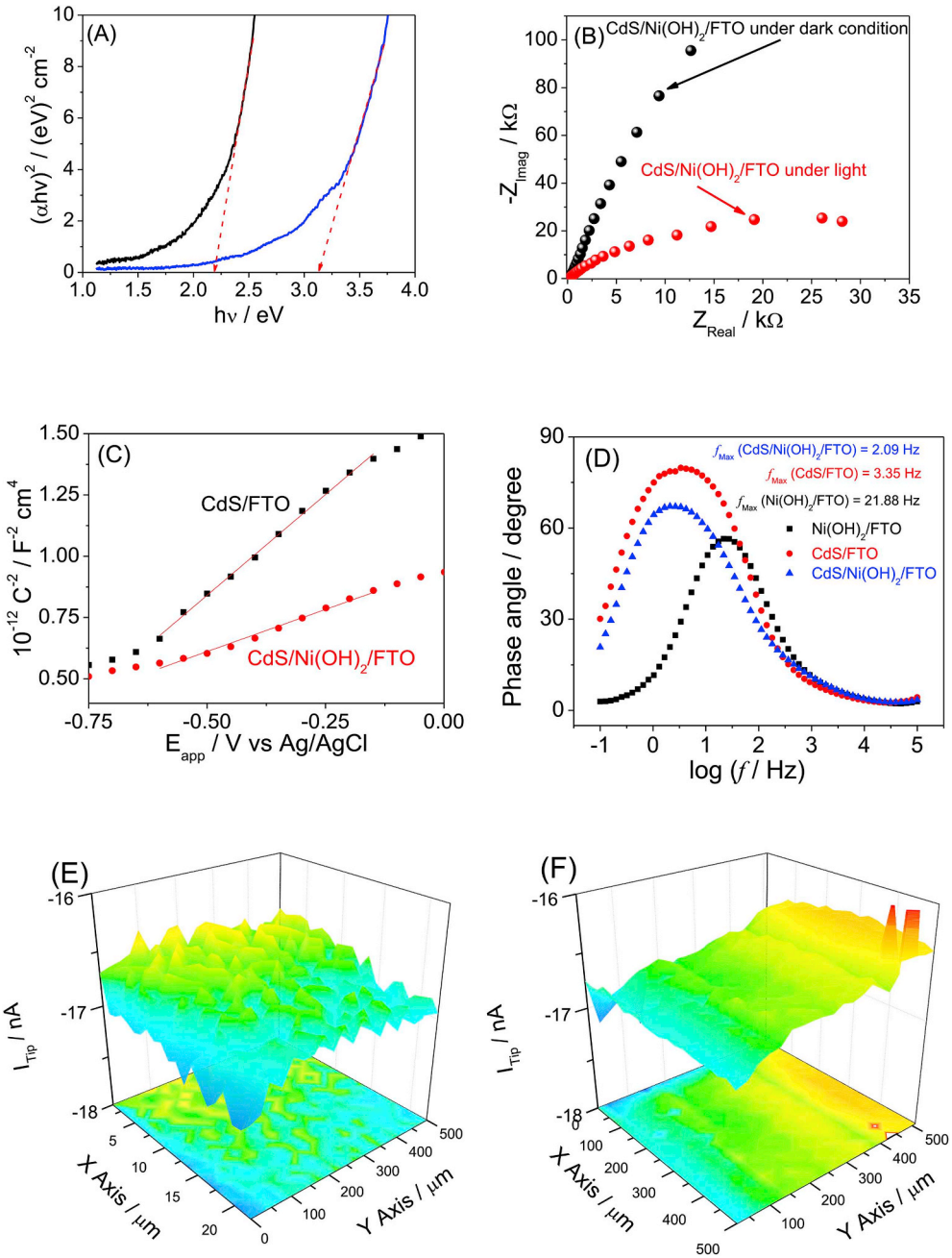

Fig. 2. (A) Plots of $(\alpha h\nu)^2$ *versus* $h\nu$ of Ni$(OH)_2$/FTO (blue line) and CdS/Ni$(OH)_2$/FTO (black line). (B) Nyquist plots of CdS/Ni$(OH)_2$/FTO photoelectrode in 0.1 mol L^{-1} Na_2SO_4 aqueous solution electrolyte recorded at room temperature and open circuit potential under dark (black circle) and visible LED light (red circle). (C) Mott-Schottky plot (C^{-2} *vs* E) for CdS/FTO (black square) and CdS/Ni$(OH)_2$/FTO (red circle) at frequency of 500 Hz. (D): Bode-phase plots for CdS/FTO (red lozenge), Ni$(OH)_2$/FTO (black square) and CdS/Ni$(OH)_2$/FTO (blue triangle) in 0.1 mol L^{-1} KCl and 0.02 mol L^{-1} ascorbic acid. (E) SECM images of CdSe/ZnS/TiO_2/FTO under incidence of light and (F) under dark obtained in 0.1 mol L^{-1} KCl aqueous solution containing 5 mmol L^{-1} of $[Fe(CN)_6]^{3-}$. The tip was biased at −200 mV *vs* Ag/AgCl while the CdS/Ni$(OH)_2$/FTO platform was maintained under OCP. (For interpretation of the references to colour in this figure legend, the reader is referred to the Web version of this article.)

under dark conditions, respectively. We highlight that the tip current for the SECM image varied according to light conditions in the photoanode. Thus, the electrode under light incidence showed significant changes, whereas there were few changes in the absence of light. As can be seen, with the CdS/Ni$(OH)_2$/FTO at open circuit potential and under incidence of light, the tip current presented a high spatial change of the tip current at some scanned regions. The following mechanism has been proposed to explain the higher and more defined tip current observed at some regions of the CdS/Ni$(OH)_2$/FTO photoelectrode under incidence of light:

$$CdS/Ni(OH)_2/FTO + h\nu \overset{\varnothing_{h\nu}}{\rightarrow} CdS^*/Ni(OH)_2/FTO$$

$$CdS^*/Ni(OH)_2/FTO \overset{k_{injection}}{\rightarrow} CdS^+/Ni(OH)_2/FTO + e^-\left(Ni(OH)_2/FTO\right)$$

$$CdS^+/Ni(OH)_2/FTO + [Fe(CN)_6]^{4-} \overset{k_{oxi}}{\rightarrow} Cd\left[S/Ni(OH)_2/FTO + \left[Fe\left(CN\right)_6\right]^{3-}\right]$$

$$[Fe(CN)_6]^{3-} \overset{tip}{\rightarrow} \left[Fe\left(CN\right)_6\right]^{4-}$$

where $\phi_{h\nu}$ represents the excitation cross-section of adsorbed sensitizer, $k_{injection}$ is the rate constant of electron injection, and k_{oxi} is the rate constant for the regenerating reaction of the sensitizer on the photocatalyst surface.

The holes generated at the surface of the CdS/Ni$(OH)_2$/FTO can regenerate the ferricyanide in a feedback operating mode of the SECM due to the higher CdS content at some regions of the film. In addition,

the SECM studies show the importance of a donor molecule on the capability of the proposed platform to produce photocurrent. Thus, the response of the platform for a donor molecule was evaluated optimizing the effects of the buffer solution on the photosensor response.

The effects of ascorbic acid (AA) as hole scavenger was evaluated in order to found the best response of the CdS/Ni(OH)$_2$/FTO photoelectrochemical platform (Fig. S1(A) and S1(B)) (*Supplementary Material*) and the effects of nature of the buffer solution and applied potential on the response of the working platform were investigated in order to found the best sensitivity of the CdS/Ni(OH)$_2$/FTO to the donor molecule (Fig. S2(A) and S2(B)) (*Supplementary Material*). The proposed photoelectrochemical sensor presented best response to the donor molecule at HEPES buffer at pH 7.4. The photoelectrode was biased at 0 V *vs* Ag/AgCl in order to avoid the necessary use of high overpotentials on the platform.

3.2. Analytical performance of PGL1M3R/CdS/Ni(OH)$_2$/FTO photoelectrochemical sensor

After the optimization of the response of the CdS/Ni(OH)$_2$/FTO photoelectrochemical platform to hole scavenger molecule, it was modified with a synthetic peptide to give the PGL1M3R/CdS/Ni(OH)$_2$/FTO photoelectrochemical sensor which was employed for the detection of anti-PGL1 in serum samples. The stepwise modification of the PGL1M3R/CdS/Ni(OH)$_2$/FTO photoelectrochemical sensor was monitored by electrochemical impedance spectroscopy (Fig. S3). (*Supplementary Material*). In order to evaluate the performance of the PGL1M3R/CdS/Ni(OH)$_2$/FTO photoelectrochemical sensor for detection of leprosy in human serum, the proposed photoelectrochemical immunosensor was incubated in the leprosy serum (positive control) and non-infected (negative sample).

Fig. 3 shows the relative photocurrent (I/I$_0$) (Fig. 3(A) and (B)) and the normalized light induced photocurrent [$\Delta I/I_o = (I_o\text{-}I)/I_o$] (Fig. 3(C)) to samples' serial dilutions (from 1:10240 to 1:40), where I$_o$ and I are the photoelectrochemical sensor photocurrent responses before and after the immune recognition. The relative current response [I/I$_0$] (Fig. 3(A) and (B)) decreases with the increase of the sample concentration while the normalized light induced current [$\Delta I/I_o = (I_o\text{-}I)/I_o$] (Fig. 3(C)) increases with the increase of the sample concentration. As can be seen, the photoelectrochemical platform was highly sensitive to leprosy patient's sera. Moreover, the non-blocked platform also showed response to negative sera samples, probably due to the presence of non-specific active sites on the platform surface. Hence, the peptide modified photoelectrochemical platform was blocked with BSA to avoid false positive results. As a consequence, the blocked PGL1M3R/CdS/Ni(OH)$_2$/FTO photoelectrochemical sensor presented different photocurrent responses for negative control compared to positive leprosy sera (Fig. 4(A-C)). Indeed, the BSA-blocked photoelectrochemical immunosensor has not presented significant responses for negative control more diluted than 1:640 (Fig. 4(A-C)). These results indicate that the novel photoelectrochemical immunosensor is a promising method for discriminating between positive and negative human sera for leprosy (Duthie et al., 2014a,b; Stefani et al., 2012).

To investigate the photoelectrochemical immunosensor selectivity, sera from tuberculosis and visceral human leishimaniasis patients were diluted to 1:640, and tested under the same conditions. These samples did not induce significant variation in the photoelectrochemical immunosensor photocurrent, revealing the device selective performance (Inset of Fig. 4(C)).

The mechanism by which the PGL1M3R/CdS/Ni(OH)$_2$/FTO photoelectrochemical sensor detects the presence of leprosy antibodies under visible LED light illumination is presented in Fig. 5. We suggest that the electrodeposited CdS on the surface of the platform captures photons promoting electrons from valence band to conducting band giving rising to e^-/h^+ pairs. Consequently, two main processes can occur. First, the electron can be injected in the Ni(OH)$_2$ to be subsequently ejected to the electrode mediating the photoelectron transfer and the hole in the valence band of the CdS can be transferred to the hole scavenger molecule. Simultaneously, the antibodies present in leprosy serum can interact with the immobilized peptides, decreasing the efficiency of the system to produce photocurrent since the peptide/leprosy antibodies interaction reduces the efficiency of the photoactive material to transfer holes to donor molecules.

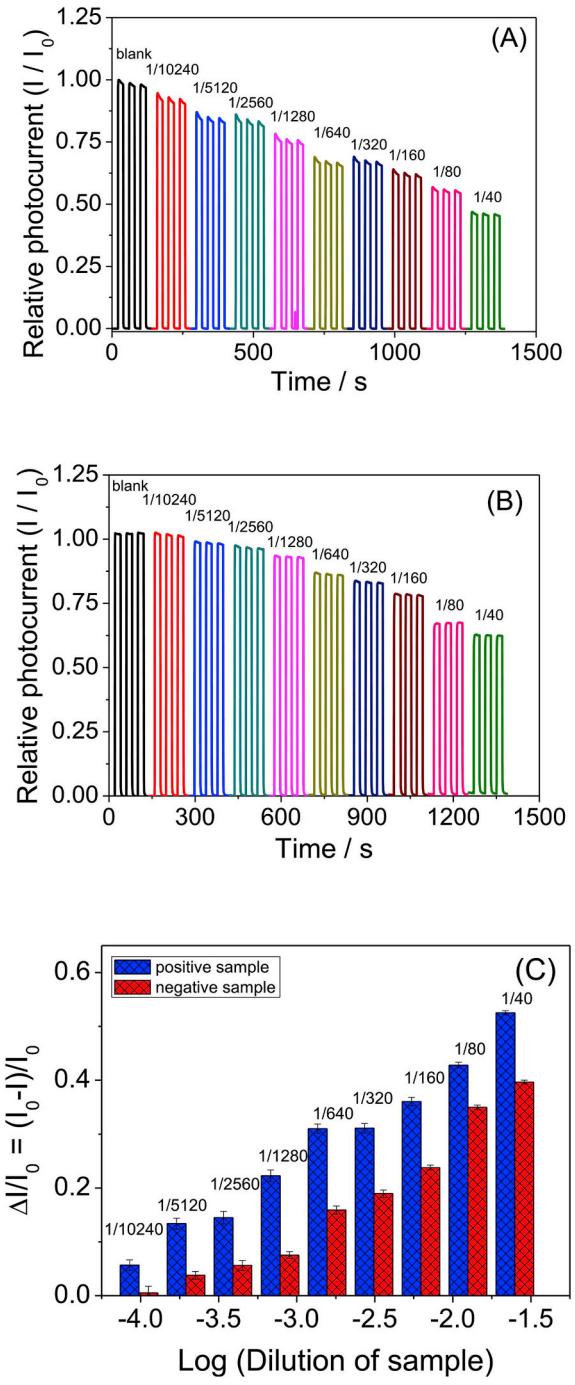

Fig. 3. Relative photocurrent responses under optimized conditions of the PGL1M3R/CdS/Ni(OH)$_2$/FTO photoelectrochemical sensor after incubated in positive (A) and negative (B) sera samples dissolved in Hepes buffer (pH 7.4) at different dilutions (v/v) (1:40, 1:80, 1:160, 1:320, 1:640, 1:1280, 1:2560, 1:5120, and 1:10240). (C) Comparison of the normalized light induced photocurrents of the immunosensor to positive (blue columns) and negative (red columns) sera samples. All measurements were performed before performing the BSA blocking step. (For interpretation of the references to colour in this figure legend, the reader is referred to the Web version of this article.)

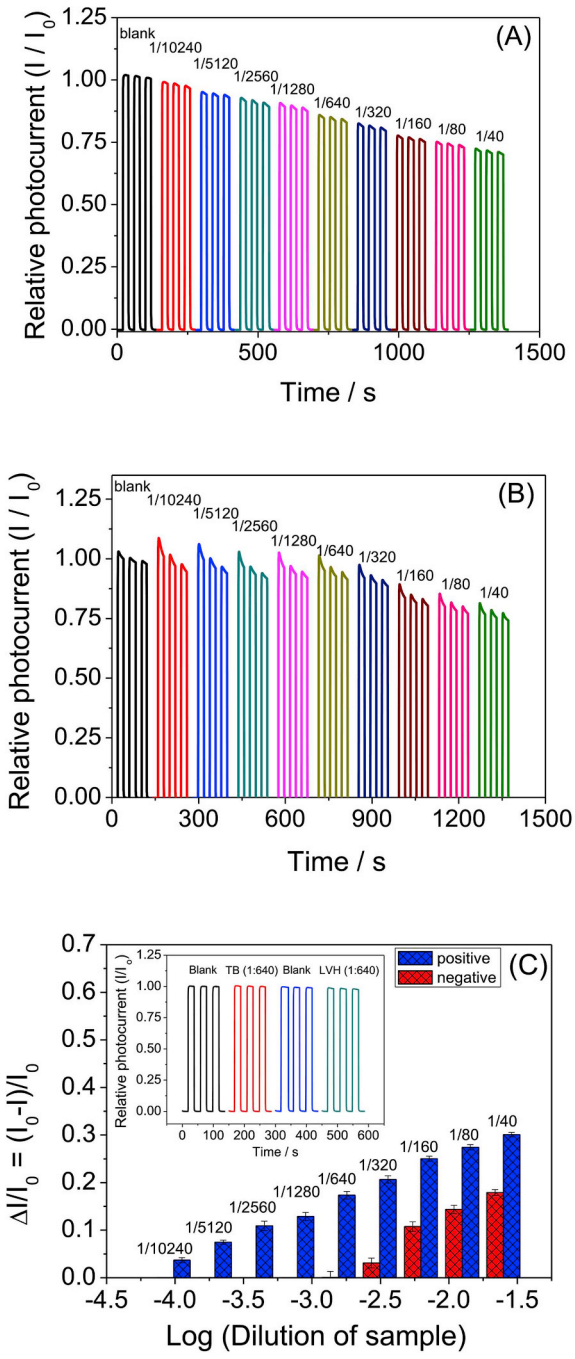

Fig. 4. Relative photocurrent responses under optimized conditions of the PGL1M3R/CdS/Ni(OH)$_2$/FTO photoelectrochemical sensor after incubated in positive (A) and negative (B) sera samples dissolved in Hepes buffer (pH 7.4) at different dilutions (v/v) (1:40, 1:80, 1:160, 1:320, 1:640, 1:1280, 1:2560, 1:5120, and 1:10240). (C) Comparison of the normalized light induced photocurrents of the immunosensor to positive (blue columns) and negative (red columns) sera samples. The inserted figure shows the photoelectrochemical response to tuberculosis (TB) and human leishmaniasis (LVH) infected samples diluted to 1:640. All measurements were performed after performing the BSA blocking step. (For interpretation of the references to colour in this figure legend, the reader is referred to the Web version of this article.)

4. Conclusions

This work reports the feasibility of electrodeposited cadmium sulfide on a nickel-based film as a low cost platform for the discrimination of positive and negative human serum samples for leprosy. The photoelectrochemical sensor shows linear response range for positive human sera samples of leprosy diluted from 1:40 up to 1:10240. The negative human sera samples for leprosy diluted lower than 1:640 does not presented significant effects on the photocurrent values indicating that the proposed photoelectrochemical sensor is a promising alternative to discriminate positive and negative samples. In addition, the photoelectrochemical sensor presented high response to positive samples for leprosy while it does not shows significant responses for sera samples infected by human leishmaniasis and tuberculosis. The present study shows the feasibility of the proposed photoelectrochemical immunosensor for the detection of leprosy contaminated samples with sensitivity and selectivity.

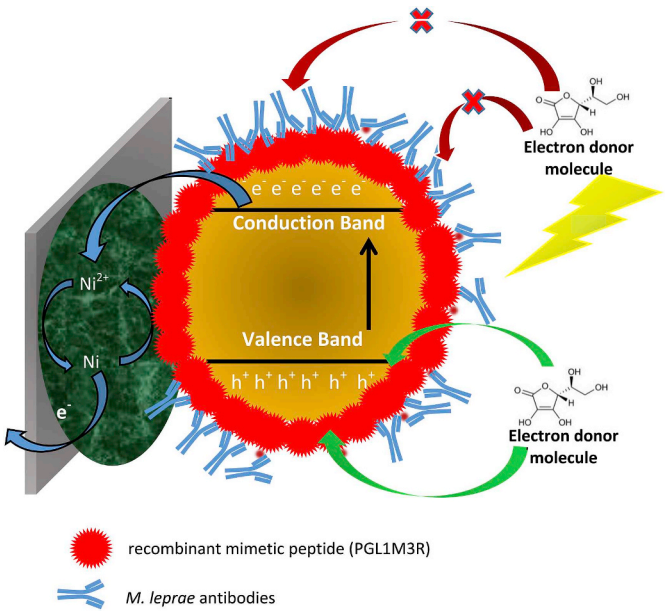

Fig. 5. Schematic representation of the proposed mechanism for the photoelectrochemical detection of anti-PGL antibodies in serum samples.

CRediT authorship contribution statement

Sakae Yotsumoto Neto: Formal analysis, Writing - original draft. **Mayara Ingrid Sousa Lima:** Supervision, Writing - review & editing. **Silma Regina Ferreira Pereira:** Supervision, Writing - review & editing. **Luiz Ricardo Goulart:** Supervision, Writing - review & editing. **Rita de Cássia Silva Luz:** Supervision, Writing - review & editing. **Flavio Santos Damos:** Supervision, Writing - review & editing.

Declaration of competing interest

The authors declare that they have no known competing financial interests or personal relationships that could have appeared to influence the work reported in this paper.

Acknowledgements

The authors are grateful to FAPEMA (PRONEM-00155/16; UNIVERSAL-00927/16; UNIVERSAL-01194/17), CNPq (303525/2016-9; 421139/2016-1; 308204/2018-2; 426337/2016-6), and INCTBio (Grant: 465389/2014-7) for financial support. The Authors are also grateful to CNPq, CAPES and FAPEMIG for providing financial support to the National Institute of Science and Technology in Theranostics and Nanobiotechnology (CNPq/CAPES/FAPEMIG, grant numbers CNPq-465669/2014-0 and FAPEMIG-CBB-APQ-03613-17). The Authors are grateful to PPSUS - FAPEMA/MS-DECIT/CNPq/SES/Nº 008/2016 (Grant number PPSUS-05972/16). The authors are grateful to the Microscopy Center/UFMG by the SEM images and EDX spectra.

Appendix A. Supplementary data

Supplementary data to this article can be found online at https://doi.org/10.1016/j.bios.2019.111625.

References

Alban, S.M., Moura, J.F., Thomaz-Soccol, V., Sékula, S.B., Alvarenga, L.M., Mira, M.T., Olortegui, C.C., Minozzo, J.C., 2014. Phage display and synthetic peptides as promising biotechnological tools for the serological diagnosis of leprosy. PLoS One 9, e106222. https://doi.org/10.1371/journal.pone.0106222.

Al-Hussam, A.M.A., Jassim, S.A.-J., 2012. Synthesis, structure, and optical properties of CdS thin films nanoparticles prepared by chemical bath technique. Basic and Applied Sciences 11, 27–31. https://doi.org/10.1016/j.jaubas.2011.10.001.

Bisquert, J., Fabregat-Santiago, J., Mora-Seró, I., Garcia-Belmonte, G., Giménez, S., 2009. Electron lifetime in dye-sensitized solar cells: theory and interpretation of measurements. J. Phys. Chem. C 113, 17278–17290. https://doi.org/10.1021/jp9037649.

Bora, D.K., Braun, A., Erni, R., Muller, U., Dobeli, M., Constable, E.C., 2013. Hematite–NiO/$Ni(OH)_2$ heterostructure photoanodes with high electrocatalytic current density and charge storage capacity. Phys. Chem. Chem. Phys. 15, 12648–12659. http://doi.org/10.1039/c3cp52179f.

Duthie, M.S., Raychaudhuri, R., Tutterrow, Y.L., Misquith, A., Bowman, J., Casey, A., Balagon, M.F., Maghanoy, A., Beltran-Alzate, J.C., Romero-Alzate, M., Cardona-Castro, N., Reed, S.G., 2014a. A rapid ELISA for the diagnosis of MB leprosy based on complementary detection of antibodies against a novel protein-glycolipid conjugate. Diagn. Microbiol. Infect. Dis. 79, 233–239. http://doi.org/10.1016/j.diagmicrobio.2014.02.006.

Duthie, M.S., Balagon, M.F., Maghanoy, A., Orcullo, F.M., Cang, M., Dias, R.F., Collovati, M., Reed, S.G., 2014b. Rapid quantitative serological test for detection of infection with Mycobacterium leprae, the causative agent of leprosy. J. Clin. Microbiol. 52, 613–619. http://doi.org/10.1128/JCM.02085-13.

Feng, K., Yang, M., Xie, F., Diao, G., Ou, M., Huang, H., 2017. TiO_2/CdS nanorod array-based photoelectrochemical sensing of Cu^{2+} in human serum samples. Anal. Methods 9, 6754–6759. http://doi.org/10.1039/C7AY02625K.

Gelderman, K., Lee, L., Donne, S.W., 2007. Flat-band potential of a semiconductor: using the Mott–Schottky equation. J. Chem. Educ. 84, 685–688. https://doi.org/10.1021/ed084p685.

Izgorodin, A., Winther-Jensen, O., Winther-Jensen, B., MacFarlane, D.R., 2009. CdS thin-film electrodeposition from a phosphonium ionic liquid. Phys. Chem. Chem. Phys. 11, 8532–8537. https://doi.org/10.1039/B906995J.

Jadhav, R., Suneetha, L., Kamble, R., Shinde, V., Devi, K., Chaduvula, M.V., Raju, R., Suneetha, S., Nicholls, P.G., van Brakel, W.H., Lockwood, D.N.J., 2011. Analysis of antibody and cytokine markers for leprosy nerve damage and reactions in the INFIR cohort in India, 2011. PLoS Neglected Trop. Dis. 5, e977. https://doi.org/10.1371/journal.pntd.0000977.

Liu, X., Jiang, H., 2017. Construction and potential applications of biosensors for proteins in clinical laboratory diagnosis. Sensors 17, e2805. https://doi.org/10.3390/s17122805.

Lobato, J., Reis, E.M., Gonçalves, M.A., Spencer, J., Brennan, P., Goulart, L.R., Goulart, I.M.B., 2011. Comparison of three immunological tests for leprosy diagnosis and detection of subclinical infection. Lepr. Rev. 82, 389–401. https://www.ncbi.nlm.nih.gov/pubmed/22439279.

Mao, L., Ba, Q., Jia, X., Liu, S., Liu, H., Zhang, J., Li, X., Chen, W., 2019. Ultrathin $Ni(OH)_2$ nanosheets: a new strategy for cocatalyst design on CdS surfaces for photocatalytic hydrogen generation. RSC Adv. 9, 1260–1269. https://doi.org/10.1039/C8RA07307D.

Ooms, M.D., Dinh, C.T., Sargent, E.H., Sinton, D., 2016. Photon management for augmented photosynthesis. Nat. Commun. 7, 1–13. e12699. https://doi.org/10.1038/ncomms12699.

Ridley, D.S., Jopling, W.H., 1962. A classification of leprosy for research purposes. Lepr. Rev. 33, 119–128. http://www.ncbi.nlm.nih.gov/pubmed/14492126.

Ridley, D.S., Jopling, W.H., 1966. Classification of leprosy according to immunity. A five-group system. Int. J. Lepr. Other Mycobact. Dis. 34, 255–273. https://www.ncbi.nlm.nih.gov/pubmed/5950347.

Rodrigues, L.C., Lockwood, D.N.J., 2011. Leprosy now: epidemiology, progress, challenges, and research gaps. Lancet Infect. Dis. 11, 464–470. https://doi.org/10.1016/S1473-3099(11)70006-8.

Rodríguez, C.A., Sandoval-Paz, M.G., Saavedra, R., Trejo-Cruz, C., De la Carrera, F., Aragon, L.E., Sirena, M., Delplancke, M.-P., Carrasco, C., 2016. Comprehensive study of growth mechanism and properties of low Zn content Cd1-xZnxS thin films by chemical bath. Math. Res. 19, 1335–1343. https://doi.org/10.1590/1980-5373-MR-2015-0660.

Stefani, M.M., Grassi, A.B., Sampaio, L.H., Sousa, A.L., Costa, M.B., Scheelbeek, P., Neupane, K.D., Hagge, D.A., Macdonald, M., Cho, S.N., Oskam, L., Bührer-Sékula, S., 2012. Comparison of two rapid tests for anti-phenolic glycolipid-I serology in Brazil and Nepal. Mem. Inst. Oswaldo Cruz 107, 124–131. https://doi.org/10.1590/S0074-02762012000900019.

Tang, Y., Traveerungroj, P., Tan, H.L., Wang, P., Amal, P., Ng, Y.H., 2015. Scaffolding an ultrathin CdS layer on a ZnO nanorod array using pulsed electrodeposition for improved photocharge transport under visible light illumination. J. Mater. Chem. 3, 19582–19587. https://doi.org/10.1039/C5TA05195A.

Vamvasakis, I., Papadas, I.T., Tzanoudakis, T., Drivas, C., Choulis, S.A., Kennou, S., Armatas, G.S., 2018. Visible-light photocatalytic H_2 production activity of β-$Ni(OH)_2$-Modified CdS mesoporous nanoheterojunction networks. ACS Catal. 8, 8726–8738. https://doi.org/10.1021/acscatal.8b01830.

Wang, X., Yan, T., Li, Y., Liu, Y., Du, B., Ma, H., Wei, Q., 2015. A competitive photoelectrochemical immunosensor based on a CdS-induced signal amplification strategy for the ultrasensitive detection of dexamethasone. Sci. Rep. 5, 1–8. 17945. https://doi.org/10.1038/srep17945.

Wang, J., Wang, Z., Zhu, Z., 2017. Synergetic effect of $Ni(OH)_2$ cocatalyst and CNT for high hydrogengeneration on CdS quantum dot sensitized TiO_2 photocatalyst. Appl. Catal. B Environ. 204, 577–583. https://doi.org/10.1016/j.apcatb.2016.12.008.

Wheeler, L., Stewart, T.J., Charlton, O.A., Crainic, O., Rosen, R., 2017. Leprosy: an ancient disease that still threatens global health. Australas. J. Dermatol. 59, 58–59. https://doi.org/10.1111/ajd.12628.

World Health Organization, 2017. Wkly. Epidemiol. Rec. 92, 501–520. http://apps.who.int/iris/bitstream/10665/258841/1/WER9235.pdf?ua=1.

Yang, S., Makredes, M., O'Donnell, P., Levin, N.A., 2013. A casa of Hansen Disease presenting as tinea versicolor. Dermatol. Online J. 19, 7. https://www.ncbi.nlm.nih.gov/pubmed/24021367.

Yotsumoto, Neto S., Silva, F.G.S., Souto, D.E.P., Faria, A.R., Andrade, H.M., Luz, R.C.S., Kubota, L.T., Damos, F.S., 2017. Photoelectrochemical immunodiagnosis of canine leishmaniasis using cadmium-sulfide-sensitized zinc oxide modified with synthetic peptides. Electrochem. Commun. 82, 75–79. https://doi.org/10.1016/j.elecom.2017.07.027.

Yotsumoto, Neto S., Souto, D.E.P., Andrade, H.M., Luz, R.C.S., Kubota, L.T., Damos, F.S., 2018. Visible LED light driven photoelectroanalytical detection of antibodies of visceral leishmaniasis based on electrodeposited CdS film sensitized with Au nanoparticles. Sens. Actuators B Chem. 256, 682–690. https://doi.org/10.1016/j.snb.2017.09.202.

Zhang, K., Lv, S., Lin, Z., Tang, D., 2017. CdS:Mn quantum dot-functionalized g-C3N4 nanohybrids as signal-generation tags for photoelectrochemical immunoassay of prostate specific antigen coupling DNAzyme concatamer with enzymatic biocatalytic precipitation. Biosens. Bioelectron. 95, 34–40. https://doi.org/10.1016/j.bios.2017.04.005.

Zhao, W.-W., Xu, J.-J., Chen, H.Y., 2015. Photoelectrochemical bioanalysis: the state of the art. Chem. Soc. Rev. 44, 729–741. https://doi.org/10.1039/C4CS00228H.